
[View Journal Online](#)
[View Article Online](#)

Investigations on spectroscopic characterizations, molecular docking, NBO, drug-Likeness, and ADME properties of 4H-1,2,4-triazol-4-amine by combined computational approach

 Sibel Celik ^{1,*} and Senay Yurdakul ²
¹ Department of Health Care Services, Ahi Evran University, Kirsehir, 40100, Turkey
sibelcelik@ahievran.edu.tr (S.C.)

² Department of Physics, Faculty of Science, Gazi University, Ankara, 06500, Turkey
senay@gazi.edu.tr (S.Y.)

 * Corresponding author at: Department of Health Care Services, Ahi Evran University, Kirsehir, 40100, Turkey.
 e-mail: sibelcelik@ahievran.edu.tr (S. Celik).

RESEARCH ARTICLE



doi: 10.5155/eurjchem.12.4.401-411.2165

Received: 29 July 2021

Received in revised form: 13 September 2021

Accepted: 14 September 2021

Published online: 31 December 2021

Printed: 31 December 2021

KEYWORDS

 DFT
 ADME
 Drug-Likeness
 Molecular docking
 Vibrational spectra
 4H-1,2,4-Triazol-4-amine

ABSTRACT

In this study, the spectroscopic characterization, frontier molecular orbital analysis, and natural bond orbital analysis (NBO) analysis were executed to determine the movement of electrons within the molecule and the stability, and charge delocalization of the 4H-1,2,4-triazol-4-amine (4-AHT) through density functional theory (DFT) approach and B3LYP/6-311++G(d,p) level of theory. Surface plots of the hybrids' Molecular Electrostatic Potential (MEP) revealed probable electrophilic and nucleophilic attacking sites. The discussed ligand were observed to be characterized by various spectral studies (FT-IR, UV-Vis). The calculated IR was found to be correlated with experimental values. The UV-Vis data of the molecule was used to analyze the visible absorption maximum (λ_{max}) using the time-dependent DFT method. Since the principle of drug-likeness is usually used in combinatorial chemistry to minimize depletion in pharmacological investigations and growth, drug-likeness and ADME properties were calculated in this research to establish 4-AHT molecule bioavailability. Furthermore, molecular docking studies were carried out. Molecular docking analysis was performed for the title ligand inside the active site of the Epidermal Growth Factor Receptor (EGFR). The title compound's anti-tumor activity against the cancer cell, in which EGFR is strongly expressed, prompted us to conduct molecular docking into the ATP binding site of EGFR to predict whether this molecule has an analogous binding mode to the EGFR inhibitors (PDB: ID: 1M17).

 Cite this: *Eur. J. Chem.* 2021, 12(4), 401-411

 Journal website: www.eurjchem.com

1. Introduction

1,2,4-Triazoles, broadly used as agricultural chemicals and pharmaceuticals [1], are synthesized in chemical coordination as a metal-azolate framework, and azole coordination polymers [1-3]. Furthermore, 1,2,4-triazoles demonstrated a wide range of bioactivities in the medicinal and agrochemical fields, resulting in a plethora of therapeutically interesting drug candidates with antimicrobial [4], anti-inflammatory [5], analgesic [6], and anticancer activities [7,8]. Due to their diverse properties, compounds containing the 1,2,4-triazole ring, such as triadimefon, triadimenol, and flusilazole, which are manufactured as commercial fungicides, may be the subject of fungicide drug research [9-12].

4H-1,2,4-Triazol-4-amine (4-AHT), a nitrogen-rich ligand, has extremely versatile coordination behavior [13]. Therefore, existing research has focused on the spectroscopic properties, synthesis, and crystal structures of complexes containing the 4-AHT molecule. A study by Dirtu [14] worked on the crystal structures and synthesis of Cu(II) [NH₂trz] mononuclear complexes. In another study, the structure and spectroscopic

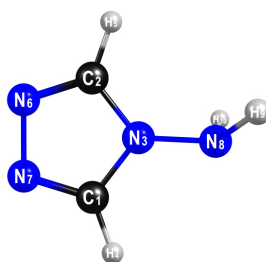
properties of the Pt (II) complex of the 4-AHT molecule were investigated using various spectroscopic techniques (IR, ¹H- and ¹³C-NMR, UV-Vis, and mass spectroscopy) [15].

As far as we know, no experimental or theoretical studies of the isolated on the ligand have been conducted. When it comes to developing structure-property relationships, the 4-AHT molecule has been extensively studied theoretically and experimentally using spectroscopic methods such as FT-IR and UV-Visible. The current work's main aim was to perform experimental and computational spectroscopic studies to better understand the title molecule's molecular geometry, vibrational modes, HOMO-LUMO, and electronic excitation. However, the NBO and NHO analyses have also been calculated and discussed in details. The bioavailability and drug-likeness screening of the title molecule was screened based on Lipinski's rule of five and ADME properties. The biological activity of the 4-AHT molecule was examined using molecular docking analysis to determine hydrogen bond length and binding energy against tyrosine kinase inhibitor (1M17) protein.

Table 1. Optimized geometrical parameters of 4-amino-4H-1,2,4-triazole obtained by B3LYP/6311G++(d,p) basis set.

Parameters	Bond lengths(Å)		Parameters	Bond angles (°)		Parameters	Dihedral angles (°)
	Calc.	XRD *		Calc.	XRD *		Calc.
C1-N3	1.367	1.335	N3-C1-H4	122.5	125.2	H4-C1-N3-C2	180.0
C1-H4	1.078	0.930	N3-C1-N7	110.3	109.7	H4-C1-N3-N8	0.0
C1-N7	1.305	1.306	H4-C1-N7	127.0	125.1	N7-C1-N3-C2	0.0
C2-N3	1.373	1.346	N3-C2-H5	123.4	125.2	N7-C1-N3-N8	-180.0
C2-H5	1.079	0.930	N3-C2-N6	110.2	109.7	N3-C1-N7-N6	0.0
C2-N6	1.305	1.297	H5-C2-N6	126.4	125.1	H4-C1-N7-N6	-180.0
N3-N8	1.401	1.419	C1-N3-C2	104.5	106.4	H5-C2-N3-C1	-180.0
N6-N7	1.386	1.382	C1-N3-N8	124.9	128.4	H5-C2-N3-N8	0.0
N8-H9	1.015	1.010	C2-N3-N8	130.5	125.0	N6-C2-N3-C1	0.0
N8-H10	1.015	1.010	C2-N6-N7	107.5	107.2	N6-C2-N3-N8	180.0
			C1-N7-N6	107.3	107.0	N3-C2-N6-N7	0.0
			N3-N8-H9	109.7	102.0	H5-C2-N6-N7	-180.0
			N3-N8-H9	109.7	98.0	C1-N3-N8-H9	-119.7
			H9-N8-H10	109.7	108.0	C1-N3-N8-H10	119.7
						C2-N3-N8-H9	60.2
						C2-N3-N8-H10	-60.2
						C2-N6-N7-C1	0.0

* X-Ray data taken from [28].

**Figure 1.** Optimized molecular structure and numbering of 4-amino-4H-1,2,4-triazole.

2. Experimental

2.1. Spectroscopic measurement

Infrared spectrum of ligand was observed between 4000 and 400 cm^{-1} on Bruker FT-IR spectrometer with ATR equipment.

2.2. Theoretical calculations

Density functional theory calculations were obtained with GAUSSIAN 09 [16] and the molecule was pictured utilizing GaussView programs [17]. The B3LYP method and B3LYP/6-311G++(d,p) basis set were used for an optimized ground-state geometry. The GaussView visualization program was used to develop the molecular electrostatic potential (MEP) surface and the frontier molecular orbitals. DOS diagram analysis was conducted using the Gauss Sum 2.2 program [18]. The absorption spectra were determined as the vertical electrical excitation energies from the ground-state structure in DMSO by time-dependent density functional theory [19]. TED (Total Energy Distribution) values were computed by means of PQS (Parallel Quantum Solutions) software [20].

The theoretical Raman intensities were calculated according to the Equation (1),

$$I_i^R = C \cdot (\nu_0 - \nu_i)^4 \cdot \nu_i^{-1} \left[1 - \exp\left(-\frac{h\nu_i c}{kT}\right) \right]^{-1} \cdot S_i^R \quad (1)$$

where ν_i is the calculated frequency of normal mode Q_i , S_i^R is the Raman scattering activity of the normal mode Q_i , C is a constant which is equal to 1×10^{-12} [21]. In this equation h , k , c , and T are Planck and Boltzmann constants, speed of light and temperature in Kelvin, respectively. ν_0 is the excitation frequency of the laser line (in this study we have used $\nu_0 = 9398.5 \text{ cm}^{-1}$ which corresponds to the wavelength of 1064 nm of a Nd:YAG laser), and I_i^R is given in arbitrary units.

The physicochemical parameters of the title compound 4-AHT were measured using Molinspiration software [22] to predict drug-likeness behavior. Drug-likeness screening and bioavailability, and pharmacokinetics profiles of the title compound were calculated by ADME properties [23] on preADMET online server [24]. Molecular docking was done on Autodock 4.2.6 software [25] and the docking results were analyzed using Discovery StudioVisualizer [26] and Pymol software [27].

3. Result and discussion

3.1. Geometry optimization

The molecular geometry of 4-AHT with atom numbering obtained by the B3LYP/6-311++G(d,p) method is shown in Figure 1. All the bond lengths and bond angle values show small deviations when compared to the calculated XRD values in Table 1. Experimental X-ray crystal data results obtained by Said [28] were used for comparison.

As seen from Figure 1, the molecular structure of 4-AHT consists of the triazole ring and the -NH₂ group. This molecule contains four C-N bonds, two N-N bonds, two C-H bonds, and two N-H bonds. The C1-H4 and C2-H5 bond lengths calculated are of the value 1.078 Å which is slightly deviated from the experimental data of a related molecule by 0.930 Å [28]. The calculated C-N bond lengths in the triazole ring are C1-N7 and C2-N6 double bonds, 1.305 Å, C1-N3 and C2-N3 single bonds, 1.367, 1.373 Å, respectively. These values are similar to the associated experimental values such as 1.306, 1.297, 1.335, and 1.346 Å. The C-N bonds reveal impartial double bond properties which are relative to the normal value of the single C-N bond (1.47 Å) and C-N bond 1.22 Å assemble given in the literature [28]. As seen in Table 1, the calculated N-H bond length in -NH₂ group varies from 1.015 Å by the B3LYP/6-311G (d,p). The corresponding values are equal experimental XRD values (1.01 Å).

Table 2. Detailed assignments of fundamental vibrations and TED of 4-amino-4H-1,2,4-triazole.

No	Mode	Calculated			Observed %TED ^c	
		Freq. ^a	I _{IR} ^b	I _{RA} ^b	IR	Assignment ^d
V ₂₄	A''	3570	16.57	37.12	-	85 ν_{NH}
V ₂₃	A''	3482	1.31	100	-	85 ν_{NH}
V ₂₂	A'	3260	0.69	57.16	3227 s	70 ν_{CH}
V ₂₁	A'	3242	0.10	40.82	3107 s	70 ν_{CH}
V ₂₀	A''	1682	24.02	6.27	1686 m	50 ν_{NH} + 26 δ_{NNH}
V ₁₉	A'	1527	37.38	7.29	1526 s	28 ν_{CN} + 14 ν_{NH} + 19 δ_{NCH} + 16 δ_{HCN}
V ₁₈	A'	1493	1.48	0.67	1454 w	25 ν_{CN} + 21 δ_{NCH} + 14 δ_{HCN}
V ₁₇	A'	1400	0.85	15.58	1379 w	52 ν_{CN}
V ₁₆	A''	1321	2.20	2.31	1316 w	34 ν_{NH} + 22 δ_{NNH} + 16 Γ_{CNNH}
V ₁₅	A'	1318	0.46	1.58	-	26 ν_{CN} + 15 ν_{NN}
V ₁₄	A'	1211	0.75	3.42	-	23 δ_{NCH} + 37 δ_{HCN}
V ₁₃	A'	1205	15.01	5.75	1194 vs	24 δ_{HCN} + 14 δ_{NCH}
V ₁₂	A'	1070	38.91	4.11	1074 vs	25 ν_{CN} + 24 δ_{NCH} + 14 δ_{NCN}
V ₁₁	A'	993	3.69	4.50	978 m	30 ν_{NN}
V ₁₀	A'	939	6.73	0.53	945 m	23 δ_{NCH} + 24 δ_{CNC} + 12 Γ_{CNNH}
V ₉	A''	882	100	1.22	873 s	16 ν_{NH} + 21 δ_{NNH} + 41 Γ_{CNNH}
V ₈	A''	832	26.16	0.05	833 s	52 Γ_{HCNN} + 21 Γ_{HCNC}
V ₇	A''	792	4.13	0.08	-	28 Γ_{HCNC} + 45 Γ_{HCNN}
V ₆	A''	688	0.50	0.18	-	13 Γ_{HCNN} + 32 Γ_{NCNN}
V ₅	A'	681	5.42	5.02	677 m	13 ν_{NN} + 20 Γ_{CNNH}
V ₄	A''	613	30.18	0.11	615 vs	15 Γ_{HCNC} + 20 Γ_{NCNC} + 26 Γ_{CNNH}
V ₃	A'	386	7.84	0.96	-	12 ν_{CN} + 47 δ_{CNC}
V ₂	A''	269	44.52	0.95	-	40 ν_{NH} + 18 Γ_{CNNH}
V ₁	A''	206	0.05	0.26	-	20 ν_{NH} + 24 Γ_{CNNH} + 11 Γ_{HCNN}

^a Scaled wavenumbers calculated at B3LYP/6-311G++(d,p) using scaling factors 0.9978.

^b Relative absorption intensities and relative Raman intensities normalized with highest peak absorption equal to 100.

^c Total energy distribution calculated B3LYP/6-311G++(d,p) level, TED less than 10% are not shown.

^d ν -stretching, δ -in-plan bending, Γ -torsion, s-strong, m-medium, w-weak, v-very.

Similarly, the bond angle computed for H-N-H in the present investigation is 109.7°, which is comparable with the corresponding experimental value of 108.0° for the related molecule given by Said *et al.* [28].

When Said *et al.* measured the X-ray data of their prepared title molecule, the maximum bond length deviation was 0.023 Å, which corresponded to the calculated findings in this paper. The experimental values are slightly higher than the optimized values, as seen in the data in the table. A possible explanation for this is that the experimental results are for molecules in a solid state with intermolecular interactions and crystal packing effects, while the theoretical measurements are for isolated molecules in a gas state.

3.2. Assignment of vibrational spectra

Experimental infrared bands, computed frequencies, intensities, and detailed assignments for the title molecule are given in Table 2. Moreover, a comparison between the experimental and theoretical FT-IR spectra was shown in Figure 2. Since non-harmonic effects are ignored in the theoretical process, the measured quantum chemical harmonic vibrational frequencies are usually greater than the fundamentals found experimentally [29-31]. In the current study, a scale factor of 0.9978 [32] was used to compare the experimental vibrational modes with the theoretical frequencies for the 4-AHT molecule.

The presence of the H, N, and C atoms in the 4-AHT molecule is obvious based on the optimized configuration and geometric parameters of the molecule. Therefore, the vibration modes that characterize C-H, N-H, C-N and N-N bonds must appear in the FT-IR spectrum of the 4-AHT.

The IR band at 3319 cm⁻¹ corresponds to the $\nu_{NH_2}^{as}$ vibration of the hydrogen-bonded. The corresponding $\nu_{NH_2}^s$ is observed as a split IR band at 3277 and 3180 cm⁻¹. This phenomenon is common in systems with asymmetric hydrogen bonding involving the primary amino group, and it is caused by the Fermi resonance splitting of the corresponding band for $\nu_{NH_2}^s$ [15]. The corresponding values for and should be 3570 and 3482 cm⁻¹, respectively.

The obtained low-frequency change of the stretching vibrations of the NH₂ group in the experimental IR spectrum is

explained by the NH₂ group's involvement in intermolecular NH...N, which is common for other NH₂-substituted heterocycles [33,35,36]. The relatively intense IR band in molecules at 1686 cm⁻¹ (medium) belongs to ν_{NH_2} (bending), while the observed maximum at 1600-1500 cm⁻¹ to the in-plane (i.p.) vibrations of the aromatic skeleton [33-36]. The experimental vibration evidence was found to be in strong harmony with the theoretical vibration.

The presence of purely C-H vibrations in the experimental FT-IR spectrum of the title molecule was shown by strong infrared bands in the 3227 cm⁻¹ (calculated at 3260 cm⁻¹, 70% TED) and 3107 cm⁻¹ (calculated at 3242 cm⁻¹, 70 % TED), respectively.

Torsion CNNH vibrations were calculated at 1321, 939, 882, 681, and 613 cm⁻¹. These infrared bands were found to be at 1316 weak (16% TED), 945 medium (12% TED), 873 strong (41% TED), 677 medium (20% TED), and 615 cm⁻¹ very strong (26% TED), respectively in the 4-AHT's experimental FT-IR spectrum.

The arrangement comprises a heterocyclic five-membered ring (1,2,4-triazole) consisting of two carbon and three nitrogen atoms [37], as determined by quantum chemical harmonic vibrational frequencies (Figure 1). Based on this, it was fair to conclude that the FT-IR spectrum of the title compound Joshi *et al.* would show a significant number of infrared bands due to C-N and N-N vibrations. Joshi *et al.* [30] reported the presence of aromatic C-N stretching absorption at 1618 cm⁻¹ in the experimental FT-IR spectrum of 4-amino-5-[N'-(2-nitrobenzylidene)-hydrazino]-2,4-dihydro-[1,2,4]-triazole-3-thione. In another work [38], C-N stretching vibrations were observed experimentally at wavenumbers of 1629 and 1528 cm⁻¹. We detected C-N stretching vibrations experimentally at 1526 (strong) and 1074 cm⁻¹ (very strong), which coincide strongly with the values calculated theoretically, 1527 (28% TED) and 1070 cm⁻¹ (25% TED), respectively. It found the presence of N-N stretching vibrations at wavenumber values of 978 and 677 cm⁻¹ (medium). These modes calculated in the infrared band at 993 and 681 cm⁻¹ with a 30% TED contribution assigned to N-N stretching vibration, can be observed in the theoretical FT-IR spectrum of 4-AHT as well (Figure 2, Table 2).

Table 3. The second order perturbation energies $E^{(2)}$ (kcal/mol) corresponding to the most important charge transfer interactions (donor-acceptor) in the compound studied by B3LYP/6-11++G(d,p) method.

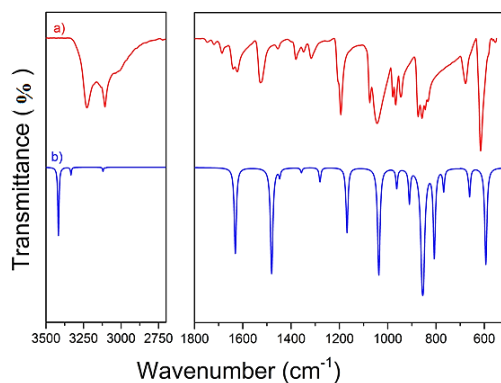
Donor NBO (i)	Acceptor NBO (j)	$E^{(2)}$ (kcal/mol) ^a	$sj-si$ (a.u.) ^b	$F(i,j)$ (a.u.) ^c
$\eta(N3)$	$\sigma^*(C2-N6)$	39.70	0.29	0.099
$\eta(N3)$	$\sigma^*(C1-N7)$	39.63	0.30	0.100
$\sigma(C1-N7)$	$\sigma^*(C2-N6)$	14.43	0.32	0.064
$\sigma(C2-N6)$	$\sigma^*(C1-N7)$	13.26	0.33	0.062
$\eta(N8)$	$\pi^*(C2-N3)$	9.23	0.80	0.077
$\eta(N6)$	$\pi^*(C2-N3)$	6.10	0.81	0.063
$\eta(N7)$	$\pi^*(C1-N3)$	5.87	0.82	0.062
$\eta(N6)$	$RY^*(C2)$	4.99	1.42	0.076
$\eta(N7)$	$\pi^*(C2-N6)$	4.92	0.96	0.062
$\eta(N7)$	$RY^*(C1)$	4.89	1.50	0.077
$\pi(C2-N6)$	$\pi^*(N3-N8)$	4.86	1.13	0.066
$\eta(N6)$	$\pi^*(C1-N7)$	4.80	0.96	0.061
$\pi(C1-N7)$	$\pi^*(N3-N8)$	4.49	1.13	0.064
$\eta(N3)$	$\pi^*(N8-H9)$	4.28	0.68	0.054
$\eta(N3)$	$\pi^*(N8-H10)$	4.28	0.68	0.054
$\pi(N6-N7)$	$\pi^*(C2-H5)$	3.98	1.17	0.061
$\pi(N6-N7)$	$\pi^*(C1-H4)$	3.83	1.18	0.06
$\pi(C1-H4)$	$\pi^*(N6-N7)$	3.13	0.95	0.049
$\pi(C2-H5)$	$\pi^*(N6-N7)$	3.08	0.96	0.049
$\eta(N3)$	$RY^*(C2)$	3.02	1.35	0.064

σ -Sigma bonds, π -Pi bonds, η : Lone pairs, RY^* : Rydberg.

^a $E^{(2)}$ means energy of hyper conjugative interactions.

^b Energy difference between donor and acceptor i and j NBO orbitals.

^c $F(i,j)$ is the Fock matrix element between i and j NBO orbitals.

**Figure 2.** Experimental (a) and theoretical (b) FT-IR spectra of 4-amino-4H-1,2,4-triazole.

3.3. Natural bond orbital analysis

Natural bond orbital (NBO) analysis can provide an exact Lewis structure of a molecule by using the highest percentage of electron density of an orbital, and it is commonly recognized as a sensitive tool for the analysis of intramolecular and intermolecular interactions since it provides information on interactions between filled and virtual orbitals [39]. The distribution of electron density is measured in atoms and in bonds between atoms by normal (localized) orbitals in the field of computer chemical chemistry.

NBO contains information such as donor (i), type, acceptor (j), occupancy, $E^{(2)}$, $\epsilon(j)-\epsilon(i)$ ^b, $F(i,j)$ ^c that $E^{(2)}$ is calculated using the formula below.

$$E^{(2)} = \Delta E_{ij} = q_i \left(\frac{F_{ij}^2}{\epsilon_j - \epsilon_i} \right) \quad (2)$$

The value of the donor orbital is q_i , the diagonal elements are ϵ_i and ϵ_j , and the off-diagonal NBO Fock matrix element is $F_{(i,j)}$. Whatever the value of $E^{(2)}$ is, it means that the atoms are interacting further.

The NBO analysis for the 4-AHT molecule was done to determine non-bonding electron pairs between atoms and their electron transfers using the B3LYP/6-311++G(d,p) method (Table 3).

The orbital overlapping between bonding and antibonding orbitals forms the title molecule intramolecular interaction

which result in intermolecular charge transfer basis electron density and device stabilization. In the present study, strong intramolecular hyper conjugative interaction was observed for the bonding orbital $\sigma(C1-N7)$ distributed to the anti-bonding orbital $\sigma^*(C2-N6)$ with a stabilization energy of 14.43 kJ/mol. It was seen that the intra-molecular interaction of $\pi \rightarrow \pi^*$ was between $\pi(C2-N6) \rightarrow \pi^*(N3-N8)$ having $E^{(2)} = 4.86$ kcal/mol. Since the π type orbitals are weaker than the σ type orbitals, resulting in lowering of electron occupancy with associated atoms. In addition, there was strong interaction between $\eta(N3) \rightarrow \sigma^*(C2-N6)$ with $E^{(2)} = 39.70$ kcal/mol [40]. Because the $E^{(2)}$ value is higher, there is more contact between electron donors and electron acceptors, i.e., the donation propensity of electron donors to electron acceptors is higher, resulting in the system's stability [41].

The natural localized molecular orbital (NLMO) analysis of the 4-AHT molecule is a significant electron overlap, as shown in Table 4, and NLMO is a slightly delocalized NBO [42]. The C1-N3 orbital with 1.9869 electrons has 35.84% C1 character in a $sp^{2.45}$ hybrid and 64.16% N2 character in a $sp^{1.87}$ hybrid. The C1-N7 orbital with 1.9828 electrons has a 42.58% C1 character in a $sp^{1.88}$ hybrid and 57.42% N7 character in a $sp^{1.78}$ hybrid (Table 4). The magnitudes of these coefficients demonstrate the significance of the two hybrids in the creation of the bond. Since nitrogen has a higher electronegativity, it has a higher percentage of NBO in the molecule and therefore a higher polarization coefficient.

Table 4. Bond orbital analysis of 4-AHT on B3LYP/6-311++G(d,p) *.

Bond (A-B)	ED energy	ED _A (%)	ED _B (%)	NBO	S _A (%)	P _A (%)	d _A (%)	S _B (%)	P _B (%)
σ(C1-N3)	1.9869	35.84	64.16	0.5986 × (sp ^{2.45}) + 0.8010 × (sp ^{1.87})	28.93	70.95	-	34.88	65.08
σ(C1-H4)	1.9828	60.74	39.26	0.7794 × (sp ^{1.73}) + 0.6266 × (sp)	36.66	63.31	-	99.94	0.06
σ(C1-N7)	1.9894	42.58	57.42	0.6525 × (sp ^{1.88}) + 0.7578 × (sp ^{1.78})	34.64	65.26	-	35.98	63.90
π(C1-N7)	1.8896	42.70	57.30	0.6535 × (sp) + 0.7570 × (sp)	0.00	99.80	-	0.00	99.82
σ(C2-N3)	1.9890	35.94	64.06	0.5995 × (sp ^{2.45}) + 0.8004 × (sp ^{1.83})	28.95	70.93	-	35.29	64.67
σ(C2-H5)	1.9833	60.31	39.69	0.7766 × (sp ^{1.75}) + 0.6300 × (sp)	36.33	63.64	-	99.94	0.06
σ(C2-N6)	1.9887	42.68	57.32	0.6533 × (sp ^{1.86}) + 0.7571 × (sp ^{1.78})	34.94	64.96	-	35.95	63.93
π(C2-N6)	1.8977	43.88	56.12	0.6624 × (sp) + 0.7491 × (sp)	0.00	99.82	-	0.00	99.82
σ(N3-N8)	1.9944	54.52	45.48	0.7383 × (sp ^{2.36}) + 0.6744 × (sp ^{2.87})	29.74	70.20	-	25.80	74.07
σ(N6-N7)	1.9738	50.14	49.86	0.7081 × (sp ^{3.12d^{0.01}}) + 0.7061 × (sp ^{3.16d^{0.01}})	24.23	75.61	0.16	24.03	75.81
σ(N8-H9)	1.9891	68.40	31.60	0.8270 × (sp ^{2.74}) + 0.5622 × (sp)	26.69	73.22	-	99.93	0.07
σ(N8-H10)	1.9891	68.40	31.60	0.8270 × (sp ^{2.74}) + 0.5622 × (sp)	26.69	73.22	-	99.93	0.07
η(N6)	1.9425	-	-	(sp ^{1.50d})	40.04	59.88	0.08	-	-
η(N7)	1.9434	-	-	(sp ^{1.48d})	40.22	59.70	0.08	-	-
σ*(C1-N3)	0.0412	64.16	35.84	0.8010 × (sp ^{2.45}) - 0.5986 × (sp ^{1.87})	28.93	70.95	-	34.88	65.08
σ*(C1-H4)	0.0172	39.26	60.74	0.6266 × (sp ^{1.73}) - 0.7794 × (sp)	36.66	63.31	-	99.94	0.06
σ*(C1-N7)	0.0148	57.42	42.58	0.7578 × (sp ^{1.88}) - 0.6525 × (sp ^{1.78})	34.64	65.26	-	35.98	63.90
π*(C1-N7)	0.3033	57.30	42.70	0.7570 × (sp) - 0.6535 × (sp)	0.00	99.80	-	0.00	99.82
σ*(C2-N3)	0.0481	64.06	35.94	0.8004 × (sp ^{2.45}) - 0.5995 × (sp ^{1.83})	28.95	70.93	-	35.29	64.67
σ*(C2-H5)	0.0178	39.69	60.31	0.6300 × (sp ^{1.75}) - 0.7766 × (sp)	36.33	63.64	-	99.94	0.06
σ*(C2-N6)	0.0160	57.32	42.68	0.7571 × (sp ^{1.86}) - 0.6533 × (sp ^{1.78})	34.94	64.96	-	35.95	63.93
π*(C2-N6)	0.3098	56.12	0.00	0.7491 × (sp)	0.00	99.82	-	0.00	0.00
σ*(N3-N8)	0.0256	45.48	54.52	0.6744 × (sp ^{2.36}) - 0.7383 × (sp ^{2.87})	29.74	70.20	-	25.80	74.07
σ*(N6-N7)	0.0164	49.86	50.14	0.7061 × (sp ^{3.12d^{0.01}}) - 0.7081 × (sp ^{3.16d^{0.01}})	24.23	75.61	0.16	24.03	75.81
σ*(N8-H9)	0.0102	31.60	68.40	0.5622 × (sp ^{2.74}) - 0.8270 × (sp)	26.69	73.22	-	99.93	0.07
σ*(N8-H10)	0.0102	31.60	68.40	0.5622 × (sp ^{2.74}) - 0.8270 × (sp)	26.69	73.22	-	99.93	0.07

* ED: occupancy, ED_A, ED_B: Percent contribution of occupancy from A and B atoms, NBO: Hybrids, S_A, P_A, S_B, P_B percentage s-character, p-character, d-character each atom.

Table 5. The NHO data obtained at B3LYP/6-311++G(d,p) level of theory for 4-AHT, which include NHO directionally and bending angles (deviations from line of nuclear centers) *.

NBO	Line of centers		Hybrid 1		Dev.	Hybrid 2		Dev.
	θ	Φ	θ	Φ		θ	Φ	
π(C1-N3)	90.0	51.2	90.0	49.4	1.8	90.0	238.5	7.3
π(C1-N7)	90.0	161.6	-	-	-	90.0	339.5	2.0
σ(C1-N7)	90.0	161.6	0	0.0	90.0	0.0	0.0	90.0
π(C2-N3)	90.0	306.6	90.0	309.8	3.2	90.0	118.0	8.6
π(C2-H5)	90.0	70.0	90.0	69.0	1.1	-	-	-
π(C2-N6)	90.0	196.5	-	-	-	90.0	18.5	2.1
σ(C2-N6)	90.0	196.5	0.0	0.0	90.0	0.0	0.0	90.0
π(N3-N8)	90.0	356.1	90.0	358.8	2.7	-	-	-
η(N3)	-	-	0.0	0.0	-	-	-	-
π(N6)	-	-	90.0	147.5	-	-	-	-
π(N7)	-	-	90.0	210.3	-	-	-	-
π(N8)	-	-	90.0	283.6	-	-	-	-
σ*(C1-N7)	90.0	161.6	0.0	0.0	90.0	0.0	0.0	90.0
σ*(C2-N6)	90.0	196.5	0.0	0.0	90.0	0.0	0.0	90.0

* θ and Φ spherical polar angles. Dev: The deviation angle from line of the centers between the bonded nuclei.

Natural hybrid orbitals (NHOs) are the product of unitary transformation of a symmetrically orthogonalized hybrid orbital based on a single atom into a regular atomic orbital (NAO). In the simple bond orbital picture, an NBO is an orbital formed from NHOs. The NBO for a localized σ-bond between atoms A and B, is defined as:

$$\sigma_{AB} = c_A h_A + c_B h_{AB} \quad (3)$$

where h_A and h_B are the natural hybrids centred on atoms A and B and c_A and c_B are the polarization coefficients for atoms A and B. The spherical polar angles theta (θ) and phi (φ) from the nucleus, as well as the deviation angle Dev from the line connecting the bonded nuclei, determine the position of each hybrid. Generally, for the sp^λ d^μ hybrids, the hybrid orientation is numerically calculated to equate to the highest angular amplitude. It is then compared to the direction of the internuclear axis to calculate the degree of bending in the bond as the deviation angle between them. In terms of the 4-AHT molecule, the NHO of the (C-N) bond is more bent away from the line of C1- N7, C2-N6 centres by 90° as a result of the conjugative effect of strong charge transfer and steric effect, while C1-N3, and C2-N3 centres deviate by 7.3 and 8.6°, respectively. A little lower bending effect of 2.0° is also noticed on the π(C1-N7), π(C2-N6) title molecule. The critical data

collected from Table 5 can be used to predict the course of geometry shifts caused by geometrical optimization.

3.4. Electronic properties

3.4.1. UV-Visible spectral analysis

The theoretical UV-Visible spectrum of the title molecule in DMSO was calculated by using the TD-DFT/B3LYP/6-311+G(d,p) method. The calculated results involving the excited electronic states, vertical excitation energies, excited electronic states, oscillator strength (f) and wavelength are presented in Table 6. The oscillator strength was used to quantify absorptivity as well as the sensitivity of an electronic transition (i.e. how strongly the particular electronic transition is allowed) [43]. The electronic transitions were assigned depending on the main contribution of molecular orbitals, with the orbital contributions of 10% being neglected. The visible absorption maxima of the title molecule correspond to electron transfers between frontier orbitals, such as conversion from HOMO to LUMO, according to molecular orbital geometry calculations. Among the absorption peaks found in the title compound's calculated UV-Vis spectrum, the bands at 159 and 152 nm were found to be significantly more intense than those at 197, 184, and 175 nm in the measured UV-Vis spectrum of

Table 6. Theoretical electronic absorption spectrum values of 4-amino-4H-1,2,4-triazole*.

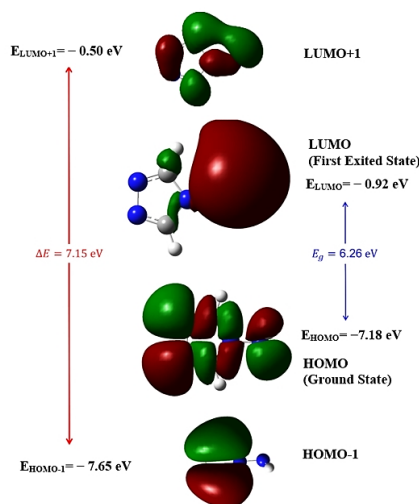
Wavelength λ (nm)	Excitation energies (eV)	Excited state	Oscillator strengths (f)
197	6.2931	(H \rightarrow L ₊₄) (H \rightarrow L ₊₅)	0.0145
189	6.5414	(H ₋₂ \rightarrow L ₊₁) (H ₋₂ \rightarrow L ₊₄) (H ₋₁ \rightarrow L ₊₁) (H ₋₁ \rightarrow L ₊₅)	0.0741
184	6.7272	(H \rightarrow L ₊₂) (H \rightarrow L ₊₃)	0.0204
175	7.0463	(H ₋₄ \rightarrow L) (H ₋₃ \rightarrow L) (H ₋₂ \rightarrow L ₊₁) (H ₋₁ \rightarrow L ₊₄)	0.0322
159	7.7776	(H ₋₁ \rightarrow L ₊₄) (39%) (H ₋₂ \rightarrow L ₊₅) (10%) (H \rightarrow L ₊₇) (20%)	0.1309
159	7.8030	(H ₋₂ \rightarrow L ₊₁) (H ₋₂ \rightarrow L ₊₄) (H ₋₁ \rightarrow L ₊₅) (H \rightarrow L ₊₇)	0.0136
154	8.0511	(H ₋₂ \rightarrow L ₊₁) (H ₋₂ \rightarrow L ₊₅) (H ₋₁ \rightarrow L ₊₄) (H ₋₁ \rightarrow L ₊₅)	0.0178
152	8.1305	(H ₋₂ \rightarrow L ₊₄) (3%) (H ₋₁ \rightarrow L ₊₅) (10%) (H \rightarrow L ₊₈) (59%)	0.0903

* H: HOMO, L: LUMO.

Table 7. The calculated HOMO-LUMO energy gaps and quantum chemical properties of title compound at DFT-B3LYP/6-311++G(d,p)*.

No	Molecular orbitals	Energy (eV)	Energy gap (eV)	I (eV)	A (eV)	η (eV)	χ (eV)	μ_c (eV)	σ (eV) ⁻¹	ω (eV) ⁻¹	$\Delta E_{\text{back-donation}}$ (eV)	
1	H	-7.18	ΔE_{H-L}	6.26	7.18	0.92	3.13	4.05	-4.05	0.32	2.62	-0.78
	L	-0.92										
2	H-1	-7.65	$\Delta E_{H-1-L+1}$	7.15	7.65	0.50	3.57	4.08	-4.08	0.28	2.33	-0.89
	L+1	-0.50										
3	H-2	-8.48	$\Delta E_{H-2-L+2}$	8.72	8.48	-0.25	4.36	4.11	-4.11	0.23	1.94	-1.09
	L+2	0.25										

* I: Ionization potential, A: Electron affinity, η : Global hardness, χ : Electronegativity, μ_c : Chemical potential, σ : Global softness, ω : Global electrophilicity, H: HOMO, L: LUMO, $I = -E_{\text{HOMO}}$, $A = -E_{\text{LUMO}}$, $\eta = \frac{(I-A)}{2}$, $\mu = \frac{-(I+A)}{2}$, $\chi = \frac{(I+A)}{2}$, $\sigma = \frac{1}{2\eta}$, $\omega = \mu^2/2\eta$.

**Figure 3.** Frontier molecular orbitals of the 4-amino-4H-1,2,4-triazole.

the compound. As a result, it was fair to conclude that transitions at wavelengths of 159 and 152 nm would have a greater chance of occurring than those at 197 and 175 nm. The first excited state (197 nm) with a transition energy of 6.2931 eV and vanishing oscillator strength of 0.0145 represents the transitions H \rightarrow L₊₄ and H \rightarrow L₊₅ (Table 6). Maximum UV-Vis radiation absorption was also observed at 159 nm with an oscillator strength of $f = 0.1309$. This absorption band orbital transition H₋₁ \rightarrow L₊₄ has a contribution of 39%. The electron transition H \rightarrow L reflects a charge transfer between the 1,2,4-triazole ring and amino group in the configuration of the 4-AHT molecule, since the HOMO and LUMO are delocalized on the cation and anion, respectively.

3.4.2. HOMO-LUMO analysis and density of state

The energy levels of molecular orbitals and density of state (DOS) were computed by the DFT-B3LYP/6-311++G(d,p) method and the diagrams of HOMO and LUMO are shown in Figure 3. The red color indicates the positive phase, while the green color indicates the negative phase, as seen in Figure 3. Furthermore, HOMO orbitals were located on the whole molecule. While LUMO orbitals have mostly been localized on the -NH₂ group and partially located on (N3-C1), (C2-H5) bonds in the triazole ring (Figure 3).

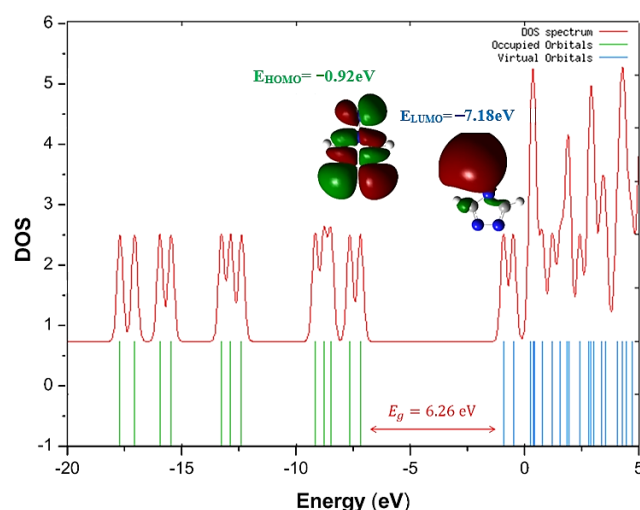
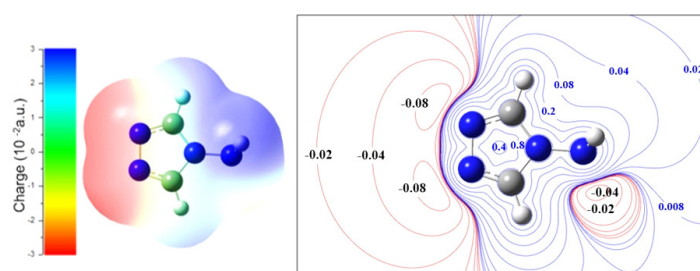
The importance of HOMO and LUMO energy can be used to describe a molecule's potential to donate and receive electrons.

Electronic and optical properties, luminescence, photochemical reactions, UV-Vis, quantum chemistry, and pharmaceutical research all benefit from understanding molecular orbitals, as well as biological processes [44-46]. The FMO's energy gap ($\Delta E_{\text{HOMO-LUMO}}$) of the described organic molecule was found to be 6.26 eV, which explains the charge transfer interactions within the molecule. Moreover, by using HOMO and LUMO energy values for 4-AHT, electron affinity (A), electronegativity (χ), ionization potential (I), chemical potential (μ_c), softness (σ), hardness (η) and electrophilicity index (ω) can be computed as their values are listed in Table 7. The chemical softness of the title molecule is 0.32 eV, while the chemical hardness is 3.13 eV, indicating that the 4-AHT molecule has strength as well as good chemical stability. The calculated value of the electrophilicity index was found to have 2.62 eV. The electrophilicity index of a molecule shows a compound's ability to bind to biomolecules [44-46]. The higher the value of the electrophilicity index of the described molecule, the greater its binding potential with biomolecules and its ability to function as an electrophilic species.

The density of states (DOS), a key concept in quantum chemistry and physics, is the number of electronic states in a unit energy interval [47]. The occupied and unoccupied molecular orbitals of the corresponding molecule are visually represented in the DOS spectrum [48]. DOS contributions reinforced the facts obtained by FMOs. The graphs of DOS calculations are shown in Figure 4.

Table 8. Comparison of NBO, Hirshfeld and APT atomic charges for title compound at B3LYP method with 6311++G(d,p) basis set.

Atoms	APT	Hirshfeld	NBO
C ₁	0.246	0.055	0.195
C ₂	0.199	0.043	0.167
N ₃	-0.165	-0.001	-0.271
H ₄	0.100	0.074	0.210
H ₅	0.087	0.069	0.200
N ₆	-0.295	-0.173	-0.297
N ₇	-0.295	-0.176	-0.306
N ₈	-0.175	-0.151	-0.622
H ₉	0.149	0.130	0.362
H ₁₀	0.149	0.130	0.362

**Figure 4.** Density of states diagram for 4-amino-4H-1,2,4-triazole.**Figure 5.** 3D and 2D molecular surface maps of 4-amino-4H-1,2,4-triazole.

3.5. Molecular electrostatic potential

The molecular electrostatic potential (MESP) surface for the 4-AHT molecule can be seen as a plot of electrostatic potential on total electron density. It depicts the distribution of charge or electron density within the molecule. Figure 5 shows MEP, 3D, and 2D contour plot maps of the 4-AHT created with the GaussView 5.0 visualization program. The varying values of the electrostatic potential are represented by varying colors. That is, blue, green, and red colors show the regions of the most positive electrostatic potential, the region of zero potential, and the regions of the most negative electrostatic potential, respectively [49]. Here, the positive electrostatic potential (blue region) is related to the repulsion of a proton by the nuclei, whereas the negative electrostatic potential (red and yellow) corresponds to the attraction of a proton by the molecule's accumulated electron density. The color range for the potential map varies from -6.562 to 6.562. As seen in Figure 5, the negative electrostatic potential (red regions) is primarily located over nitrogen atoms (N6-N7), which are the most reactive sites for an electrophilic attack, while the positive electrostatic potential (blue region) is primarily located around

the -NH₂ group, which is the most reactive location for a nucleophilic attack.

3.6. Charge analysis and Fukui functions

The molecule's charge distribution has a major effect on the vibrational spectra. The Hirshfeld, APT, and NBO atomic charges and Fukui functions of the 4-AHT molecule were calculated by the computational method of DFT/B3LYP with a 6-311++G(d,p) basis set. Atomic charge distribution research reveals the magnitude of individual net charges exhibited by atoms. Calculated atomic charge results are shown in Table 8.

It showed in the table that the nitrogen atoms had negative charge and the calculated amount of negative charge for atoms N6, N7 was more than all and it was equal to -0.295 (in APT). The triazole ring's nitrogen atom N3, which is directly attached to the amino group, has the lowest negative charge in the ring. However, carbon atoms C1 and C2 had a positive charge because they were present in the C-N structure. As a result, nitrogen's electronegativity was greater than carbon's, and it absorbed electrons into itself.

Table 9. Condensed Fukui functions calculated from Hirshfeld charges.

Atoms	f^+	f^-	f^0	f^+/f^-	f/f^+
C ₁	0.187	0.028	0.115	0.143	0.234
C ₂	0.187	0.029	0.127	0.118	0.364
N ₃	0.046	-0.002	0.022	0.048	-0.044
H ₄	0.072	0.040	0.056	0.031	0.565
H ₅	0.072	0.035	0.104	-0.063	0.486
N ₆	0.154	0.033	0.094	0.121	0.215
N ₇	0.169	0.037	0.103	0.132	0.218
N ₈	0.043	0.039	0.039	0.006	0.847
H ₉	0.033	0.299	0.166	-0.265	8.865
H ₁₀	0.033	0.299	0.166	-0.265	8.865

Table 10. Probabilities for ADME and Drug-Likeness properties of 4-amino-4H-1,2,4-triazole.

Compound	HBD	HBA	TPSA	GI absorption	BBB	Caco2 permeability	HIA	Bioavailability score
4-AHT	2	4	56.74	High	No	9.29	88.32	0.55

* HBD: Hydrogen Bond Donor, HBA: Hydrogen bond acceptor, MR: Molar refractivity, TPSA: Topological polar surface area, BBB: blood-brain barrier penetration.

Fukui functions are related to the frontier orbital principle in part because it addresses how nucleophiles attract the HOMO while depositing their excess electrons in the LUMO [50]. Fukui functions are evaluated based on the finite difference (FD) methodology for the molecule for neutral, cationic and anionic charge values of optimized molecular geometry.

The Fukui functions are calculated by the following equations [51]:

$$f_j^+ = q_k(N+1) - q_k(N) \text{ for nucleophilic attack} \quad (4)$$

$$f_j^- = q_k(N) - q_k(N-1) \text{ for electrophilic attack} \quad (5)$$

$$f_j^0 = (1/2) [q_k(N+1) - q_k(N-1)] \text{ for neutral (radical) attack} \quad (6)$$

In these equations q_k is the atomic charges and (N), (N-1), (N+1) are the neutral, cationic and anionic species of the molecule. The highest value of the (f_j^+/f_j^-) ratio is relative electrophilicity and the highest value of the (f_j^-/f_j^+) ratio is relative nucleophilicity.

The calculated Fukui functions for title molecule are presented in Table 9. According to the data provided within the table, f_j^+ value of carbon atoms and f_j^- value of amino group have maximum values. According to the equations, C1 and C2 atoms are the most prone to nucleophilic attack, while N8 atoms are the most prone to electrophilic attack in the title molecule (Table 9). The Fukui function analysis findings align well with the MEP and charge distribution results.

3.7. Drug-Likeness and ADME Analysis

The 4-AHT molecule has been tested for drug-likeness and ADME parameters in order to assess its ability for use as an active component in many novel pharmaceutical products. The pharmacokinetic parameters of absorption, delivery, metabolism, and excretion of a living body can be studied using drug-likeness data [52]. The computed values of drug-likeness and ADME parameters have been summarized in Table 10 should take values according to Lipinski's rule of five [53]. According to the Lipinski rule of five (MW < 500, (milogP) must be ≤ 5 , number of H bond donors must be ≤ 10 and H bond acceptors must be ≤ 10 , any chemical compound as an oral drug would be biologically active provided it did not break more than one of the suggested laws, commonly known as Pfizer's law of five. The octanol/water partition coefficient (milogP) values of any substance determine its hydrophilicity, which determines toxicity, absorption, and drug-receptor interactions. The data of milogP not visible in the table was calculated as 1.16. In addition, TPSA (Total polar surface area) (≤ 140) in the acceptable range [54,55]. The drug-likeness parameters obtained in this study met Lipinski's rule of five.

The acceptable range of Blood-brain barrier penetration (BBB) for an ideal drug candidate, in accordance with its entry into the central nervous system, is 0.73-0.91 [56], which indicates that this molecule is 0.180 not in the acceptable range. The negative Kp value (-7.40) indicated poor skin permeability resulting in good oral absorption. In the event of accidental contact with skin, no effect will be observed. The PPB value was less than 90 %. The bioavailability score was found to be 0.55. In terms of bioavailability, drug likeness behavior is critical for becoming an oral drug. The HIA value indicated good oral absorption of the compound. The Caco-2 (colorectal carcinoma) cell permeability values were between 4-70 considered moderately permeable. Analysis of these results shows that compounds were predicted to have human intestinal absorption (HIA) and Caco-2 (colorectal carcinoma) cell permeability.

When the physicochemical properties of the molecule found by the Lipinski's rule are combined with the ADME results, it has good drug-likeness properties. These results definitely support the pharmaceutical potential of the title molecule.

3.8. Molecular docking

1,2,4-triazole derivatives have anticancer and EGFR inhibitory activities [57]. The epidermal growth factor receptor (EGFR) is an ErbB family receptor tyrosine kinase (RTK) [2]. Aberrant activity of EGFR has been observed in various human cancers, such as non-small cell lung cancer (NSCLC), head and neck cancer, breast cancer, and colorectal cancer. Also, EGFR has a more selective role and could be a preferred target for anticancer agents. The title compound will be molecular docked within the active site of EGFR to confirm its possible mode of action within the enzyme. To demonstrate the active compound's anti-cancer activity, the 4-AHT molecule was docked against the ATP-active sites of EGFR using the 3D protein structure (PDB ID: 1M17) retrieved from the protein data bank for EGFR [58,59]. The Ramachandran plot is used to check the protein's quality. As seen in Figure 6, all residues are present within the permitted region.

A molecular docking study was performed to determine the existence of the inter-molecular interactions between the target protein (1M17) and the ligand compound. The study of protein-ligand interactions is critical in structurally based drug design. Molecular docking tests yielded binding energy, full fitness score, hydrogen bond location and length values of each ligand-protein pair. The binding energy value against anticancer protein is -6.07, indicating that the drug has a high affinity to bind and is highly active. Also, the full fitness score of the docked structure was found to be -2206.43 kcal/mol.

Figure 7 showed amino acid residues that have H-bond interactions with the ligands. The 3D and 2D diagrams showed the binding sites of the ligands within the macromolecule 1M17 (Figures 7 and 8).

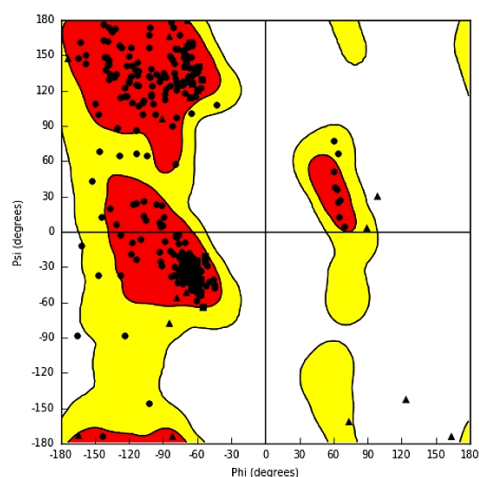


Figure 6. Ramachandran plot of 1M17 to find the quality of the protein.

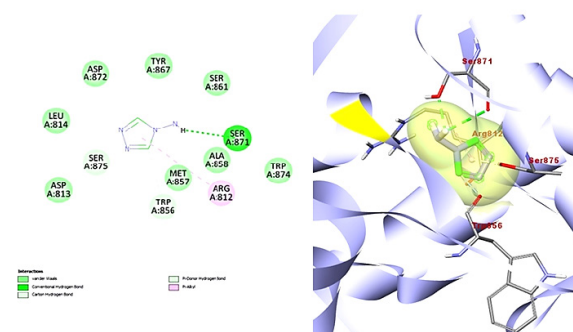


Figure 7. (a) 2D model of interaction between amino acid residues and ligand with types of bond (b) 3D model of 4-AHT ligand bonded with active site of EGFR receptor

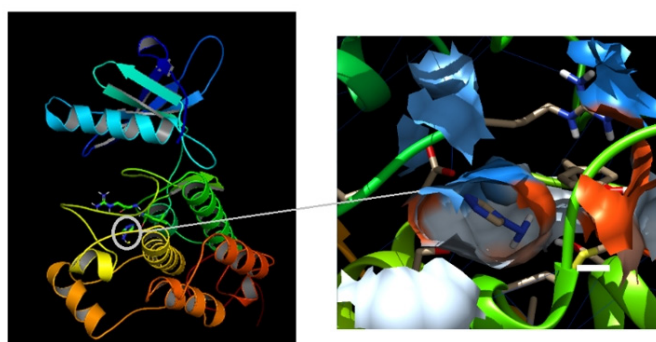


Figure 8. (a) Molecular docked model of 4-AHT ligand into the active site of EGFR (b) The hydrophobic surface model of the compound with EGFR (PDB code: 1M17) obtained by PyMOL Software.

As can be seen from the results, the hydrogen bonding of the active site of residues was demonstrated. The computed results show that LEU 814, ALA 858, SER 861, SER 871, SER 875 amino acids form a hydrogen bond interaction with bond length of 2.96, 2.69, 2.16, 2.88, 1.97 Å, respectively. The N7 of the triazole ring and the amino group were the most important for formation of the hydrogen bonds. SER814 forms two H bonds with N in the triazole ring. In addition, SER875, an H bond with N in the triazole ring, and SER861 interactions with amine group are important interactions for protein of PDB ID:1M17. ARG 812 amino acid interact with the molecule's triazole ring via a pi-alkyl (3.47 Å) interaction. In protein-ligand interactions, bond length < 3 Å indicates a strong hydrogen bond interaction

[60]. This analysis shows that the 4-AHT molecule may indicate inhibitory activity against protein inhibitors.

4. Conclusions

The experimental geometric parameters of 4-AHT in the literature agree with the values calculated by the DFT method. Simultaneously, it was discovered that the experimentally recorded FT-IR spectra were well compatible with the calculated vibration waves. The UV-Vis study absorption maximum of the title molecule corresponds to electron transfers between frontier orbitals, such as conversion from HOMO to LUMO, according to molecular orbital geometry calculations. Among the absorption peaks revealed in the title

compound's calculated UV-Vis spectrum, the bands at 159 and 152 nm were found to be significantly intense. The identified HOMO-LUMO energy gap was discovered to be 6.26 eV, which explains the charge transfer relationships within the molecule. The calculated softness and hardness values of the 4-AHT molecule indicate that it has good chemical stability as well as molecule strength. According to the MEP diagram, the NH₂ group has the highest positive potential, while the predominantly located over nitrogen atoms (N6-N7) have the highest negative potential in the corresponding area, which is the most reactive for a nucleophilic attack. The NBO analysis has identified significant intramolecular charge transfer interactions in the molecule, all kinds of interactions. The calculated drug-likeness and ADME properties demonstrated that the physicochemical properties of the title molecule follow Lipinski's rule. Also, these results show that this molecule has considerable pharmaceutical potential. Finally, the interactions between 4-AHT and the EGFR protein demonstrate that the electrostatic, hydrophobic, and hydrogen bonds, as well as the binding energy values, suggest that the ligand bind to the EGFR protein and that the 4-AHT molecule has pharmacological properties.

Disclosure statement

Conflict of interests: The authors declare that they have no conflict of interest.

Ethical approval: All ethical guidelines have been adhered.

Sample availability: Samples of the compounds are available from the author.

Availability of data and material: Available on request.

Code availability: Available on request.

CRedit authorship contribution statement

Conceptualization: Sibel Celik, Senay Yurdakul; Methodology: Sibel Celik, Senay Yurdakul; Software: Sibel Celik; Validation: Sibel Celik, Senay Yurdakul; Formal Analysis: Sibel Celik; Investigation: Sibel Celik; Resources: Senay Yurdakul; Data Curation: Sibel Celik, Senay Yurdakul; Writing - Original Draft: Sibel Celik, Senay Yurdakul; Writing - Review and Editing: Sibel Celik; Visualization: Sibel Celik.

ORCID

Sibel Celik

 <https://orcid.org/0000-0002-4852-3826>

Senay Yurdakul

 <https://orcid.org/0000-0001-9972-4444>

References

- Haasnoot, J. G. *Coord. Chem. Rev.* **2000**, 200–202, 131–185.
- Zhang, J.-P.; Zhang, Y.-B.; Lin, J.-B.; Chen, X.-M. *Chem. Rev.* **2012**, 112 (2), 1001–1033.
- Naik, A. D.; Dirtu, M. M.; Railliet, A. P.; Marchand-Brynaert, J.; Garcia, Y. *Polymers (Basel)* **2011**, 3 (4), 1750–1775.
- El-Sherief, H. A.; Abuo-Rahma, G. E.-D. A.; Shoman, M. E.; Beshr, E. A.; Abdel-baky, R. M. *Med. Chem. Res.* **2017**, 26 (12), 3077–3090.
- El Shehry, M. F.; Abu-Hashem, A. A.; El-Telbani, E. M. *Eur. J. Med. Chem.* **2010**, 45 (5), 1906–1911.
- Mathew, V.; Keshavayya, J.; Vaidya, V. P.; Giles, D. *Eur. J. Med. Chem.* **2007**, 42 (6), 823–840.
- Holla, B. S.; Poojary, K. N.; Rao, B. S.; Shivananda, M. K. *Eur. J. Med. Chem.* **2002**, 37 (6), 511–517.
- Padmavathi, V.; Sudhakar Reddy, G.; Padmaja, A.; Kondaiah, P.; Ali-Shazia. *Eur. J. Med. Chem.* **2009**, 44 (5), 2106–2112.
- Liu, X.-H.; Pan, L.; Tan, C.-X.; Weng, J.-Q.; Wang, B.-L.; Li, Z.-M. *Pestic. Biochem. Physiol.* **2011**, 101 (3), 143–147.
- Ohno, N.; Fujimoto, K.; Okuno, Y.; Mizutani, T.; Hirano, M.; Itaya, N.; Honda, T.; Yoshioka, H. *Agric. Biol. Chem.* **1974**, 38 (4), 881–883.
- Liu, X. H.; Weng, J. Q.; Tan, C. X.; Pan, L.; Wang, B. L.; Li, Z. M. *Asian J. Chem.* **2011**, 23, 4031–4036.
- Xue, Y. L.; Zhang, Y. G.; Liu, X. H. *Asian J. Chem.* **2012**, 24, 5087–5089.
- Bräunlich, I.; Medvedev, M.; Dshemuchadse, J.; Wörle, M.; Caseri, W. Z. *Angew. Chem.* **2015**, 641 (12–13), 2344–2349.
- Dirtu, M. M.; Boland, Y.; Gillard, D.; Tinant, B.; Robeyns, K.; Safin, D. A.; Devlin, E.; Sanakis, Y.; Garcia, Y. *Int. J. Mol. Sci.* **2013**, 14 (12), 23597–23613.
- Kavlakova, M.; Bakalova, A.; Momekov, G.; Ivanov, D. *J. Coord. Chem.* **2010**, 63 (20), 3531–3540.
- Frisch, M. J.; Trucks, G. W.; Schlegel, H. B.; Scuseria, G. E.; Robb, M. A.; Cheeseman, J. R.; Montgomery, J. A.; Vreven, T.; Kudin, K. N.; Burant, J. C.; Millam, J. M.; Iyengar, S. S.; Tomasi, J.; Barone, V.; Mennucci, B.; Cossi, M.; Scalmani, G.; Rega, N.; Petersson, G. A.; Nakatsuji, H.; Hada, M.; Ehara, M.; Toyota, K.; Fukuda, R.; Hasegawa, J.; Ishida, M.; Nakajima, T.; Honda, Y.; Kitao, O.; Nakai, H.; Klene, M.; Li, X.; Knox, J. E.; Hratchian, H. P.; Cross, J. B.; Adamo, C.; Jaramillo, J.; Gomperts, R.; Stratmann, R. E.; Yazyev, O.; Austin, A. J.; Cammi, R.; Pomelli, C.; Ochterski, J. W.; Ayala, P. Y.; Morokuma, K.; Voth, G. A.; Salvador, P.; Dannenberg, J. J.; Zakrzewski, V. G.; Dapprich, S.; Daniels, A. D.; Strain, M. C.; Farkas, O.; Malick, D. K.; Rabuck, A. D.; Raghavachari, K.; Foresman, J. B.; Ortiz, J. V.; Cui, Q.; Baboul, A. G.; Clifford, S.; Cioslowski, J.; Stefanov, B. B.; Liu, G.; Liashenko, A.; Piskorz, P.; Komaromi, I.; Martin, R. L.; Fox, D. J.; Keith, T.; Al-Laham, M. A.; Peng, C. Y.; Nanayakkara, A.; Challacombe, M.; Gill, P. M. W.; Johnson, B.; Chen, W.; Wong, M. W.; Gonzalez, C.; Pople, J. A. Gaussian 09, Inc., Wallingford CT, 2009.
- GaussView, Version 5, Dennington, R.; Keith, T. A.; Millam, J. M. Semichem Inc., Shawnee Mission, KS, 2009.
- O'Boyle, N. M.; Tenderholt, A. L.; Langner, K. M. *J. Comput. Chem.* **2008**, 29 (5), 839–845.
- Amat, A.; Clementi, C.; De Angelis, F.; Sgamellotti, A.; Fantacci, S. *J. Phys. Chem. A* **2009**, 113 (52), 15118–15126.
- PQS Version 3.1, Parallel Quantum Solutions, 2013 Green Acres Road, Fayetteville, Arkansas, AR72703, USA.
- Yurdakul, Ş.; Tanrıbuuyurdu, S. *J. Mol. Struct.* **2013**, 1052, 57–66.
- Molinspiration Cheminformatics free web services, <https://www.molinspiration.com>, Slovensky Grob, Slovakia (accessed Sep 10, 2021).
- Lipinski, C. A.; Lombardo, F.; Dominy, B. W.; Feeney, P. J. *Adv. Drug Deliv. Rev.* **2012**, 64 (SUPPL.), 4–17.
- Bioinformatics and Molecular Design Research Center, Seoul, South Korea, PreADMET program, 2004. Available from: URL: <http://preadmet.bmdrc.org> (accessed Sep 10, 2021).
- Morris, G. M.; Goodsell, D. S.; Halliday, R. S.; Huey, R.; Hart, W. E.; Belew, R. K.; Olson, A. J. *J. Comput. Chem.* **1998**, 19 (14), 1639–1662.
- BIOVIA, Dassault Systèmes, Discovery Studio Visualizer, v17.2.0.16349, San Diego: Dassault Systèmes, 2016.
- De Lano, W. L.; Carlos, D. L. S.; California, U. S. A. PyMOL: An open-source molecular graphics tool http://legacy.ccp4.ac.uk/newsletters/newsletter40/11_pymol.pdf (accessed Sep 14, 2021).
- Said, M.; Boughzala, H. *Acta Crystallogr. E Crystallogr. Commun.* **2018**, 74 (Pt 2), 147–150.
- Singh, H.; Singh, A.; Khurana, J. M. *J. Mol. Struct.* **2017**, 1147, 725–734.
- Joshi, R.; Pandey, N.; Yadav, S. K.; Tilak, R.; Mishra, H.; Pokharia, S. *J. Mol. Struct.* **2018**, 1164, 386–403.
- Droz, M. *J. Mol. Struct.* **2018**, 1155, 776–788.
- Bytheway, I.; Wong, M. W. *Chem. Phys. Lett.* **1998**, 282 (3–4), 219–226.
- Koleva, B. B.; Kolev, T.; Seidel, R. W.; Spittler, M.; Mayer-Figge, H.; Sheldrick, W. S. *J. Phys. Chem. A* **2009**, 113 (13), 3088–3095.
- Kolev, T.; Koleva, B. B.; Seidel, R. W.; Spittler, M.; Sheldrick, W. S. *Cryst. Growth Des.* **2009**, 9 (8), 3348–3352.
- Ivanova, B. B.; Mayer-Figge, H. *J. Coord. Chem.* **2005**, 58 (8), 653–659.
- Koleva, B. B.; Trendafilova, E. N.; Arnaudov, M. G.; Sheldrick, W. S.; Mayer-Figge, H. *Transit. Met. Chem.* **2006**, 31 (7), 866–873.
- Tankov, I.; Yankova, R. *J. Mol. Struct.* **2019**, 1179, 581–592.
- Tamer, Ö.; Bhatti, M. H.; Yunus, U.; Nadeem, M.; Avci, D.; Atalay, Y.; Yaqub, A.; Quershi, R. *J. Mol. Struct.* **2017**, 1133, 329–337.
- Chai, J.-D.; Head-Gordon, M. *J. Chem. Phys.* **2008**, 128 (8), 084106.
- Khajehzadeh, M.; Moghadam, M. *Spectrochim. Acta A Mol. Biomol. Spectrosc.* **2017**, 180, 51–66.
- Amul, B.; Muthu, S.; Raja, M.; Sevvanthi, S. *J. Mol. Struct.* **2019**, 1195, 747–761.
- Ramesh, P.; Lydia Caroline, M.; Muthu, S.; Narayana, B.; Raja, M.; Aayisha, S. *J. Mol. Struct.* **2020**, 1200 (127123), 127123.
- Srivastava, A. K.; Kumar, A.; Misra, N.; Manjula, P. S.; Sarojini, B. K.; Narayana, B. *J. Mol. Struct.* **2016**, 1107, 137–144.
- Alyar, S.; Şen, T.; Özmen, Ü. Ö.; Alyar, H.; Adem, Ş.; Şen, C. *J. Mol. Struct.* **2019**, 1185, 416–424.
- Mondal, S.; Mandal, S. M.; Mondal, T. K.; Sinha, C. *Spectrochim. Acta A Mol. Biomol. Spectrosc.* **2015**, 150, 268–279.
- Banupriya, G.; Sribalan, R.; Padmini, V. *J. Mol. Struct.* **2018**, 1155, 90–100.
- Pangh, A.; Behzadi, H.; Ghaemi, M.; Sadani, S. *Comput. Theor. Chem.* **2019**, 1155, 47–55.

- [48]. Sivaprakash, S.; Prakash, S.; Mohan, S.; Jose, S. P. *Heliyon* **2019**, 5 (7), e02149.
- [49]. Barim, E.; Akman, F. *J. Mol. Struct.* **2019**, 1195, 506–513.
- [50]. Santhy, K. R.; Sweetlin, M. D.; Muthu, S.; Kuruvilla, T. K.; Abraham, C. S. *J. Mol. Struct.* **2019**, 1177, 401–417.
- [51]. Celik, S.; Alp, M.; Yurdakul, S. *Spectrosc. Lett.* **2020**, 53 (4), 234–248.
- [52]. Zhang, Y.; Zhang, X.; Qiao, L.; Ding, Z.; Hang, X.; Qin, B.; Song, J.; Huang, J. *J. Mol. Struct.* **2019**, 1176, 335–345.
- [53]. Lipinski, C. A. *Drug Discov. Today Technol.* **2004**, 1 (4), 337–341.
- [54]. Lipinski, C. A.; Lombardo, F.; Dominy, B. W.; Feeney, P. J. *Adv. Drug Deliv. Rev.* **1997**, 23 (1–3), 3–25.
- [55]. Aayisha, S.; Renuga Devi, T. S.; Janani, S.; Muthu, S.; Raja, M.; Sevvanthi, S. *J. Mol. Struct.* **2019**, 1186, 468–481.
- [56]. Belkhir-Talbi, D.; Makhloufi-Chebli, M.; Terrachet-Bouaziz, S.; Hikem-Oukacha, D.; Ghemmit, N.; Ismaili, L.; M.S Silva, A.; Hamdi, M. *J. Mol. Struct.* **2019**, 1179, 495–505.
- [57]. El-Sherief, H. A. M.; Youssif, B. G. M.; Bukhari, S. N. A.; Abdel-Aziz, M.; Abdel-Rahman, H. M. *Bioorg. Chem.* **2018**, 76, 314–325.
- [58]. Stamos, J.; Sliwkowski, M. X.; Eigenbrot, C. *J. Biol. Chem.* **2002**, 277 (48), 46265–46272.
- [59]. Abdelazeem, A. H.; El-Saadi, M. T.; Said, E. G.; Youssif, B. G. M.; Omar, H. A.; El-Moghazy, S. M. *Bioorg. Chem.* **2017**, 75, 127–138.
- [60]. Sangeetha Margreat, S.; Ramalingam, S.; Sebastian, S.; Xavier, S.; Periandy, S.; Daniel, J. C.; Maria Julie, M. *J. Mol. Struct.* **2020**, 1200 (127099), 127099.



Copyright © 2021 by Authors. This work is published and licensed by Atlanta Publishing House LLC, Atlanta, GA, USA. The full terms of this license are available at <http://www.eurjchem.com/index.php/eurjchem/pages/view/terms> and incorporate the Creative Commons Attribution-Non Commercial (CC BY NC) (International, v4.0) License (<http://creativecommons.org/licenses/by-nc/4.0>). By accessing the work, you hereby accept the Terms. This is an open access article distributed under the terms and conditions of the CC BY NC License, which permits unrestricted non-commercial use, distribution, and reproduction in any medium, provided the original work is properly cited without any further permission from Atlanta Publishing House LLC (European Journal of Chemistry). No use, distribution or reproduction is permitted which does not comply with these terms. Permissions for commercial use of this work beyond the scope of the License (<http://www.eurjchem.com/index.php/eurjchem/pages/view/terms>) are administered by Atlanta Publishing House LLC (European Journal of Chemistry).